Chemical Science

ROYAL SOCIETY OF CHEMISTRY

EDGE ARTICLE

View Article Online
View Journal | View Issue

Cite this: *Chem. Sci.*, 2024, **15**, 3980

All publication charges for this article have been paid for by the Royal Society of Chemistry

Received 20th October 2023
Accepted 5th February 2024

DOI: 10.1039/d3sc05595g

rsc.li/chemical-science

What defines electrophilicity in carbonyl compounds†

F. Matthias Bickelhaupt *[abc] and Israel Fernández *[d]

The origin of the electrophilicity of a series of cyclohexanones and benzaldehydes is investigated using the activation strain model and quantitative Kohn–Sham molecular orbital (MO) theory. We find that this electrophilicity is mainly determined by the electrostatic attractions between the carbonyl compound and the nucleophile (cyanide) along the entire reaction coordinate. Donor–acceptor frontier molecular orbital interactions, on which the current rationale behind electrophilicity trends is based, appear to have little or no significant influence on the reactivity of these carbonyl compounds.

Introduction

The terms electrophile and nucleophile, coined by Ingold[1] based on the earlier definitions by Lewis and Weehler,[2] constitute a pivotal concept in chemistry. An electrophile typically refers to a species able to form a chemical bond by accepting an electron pair from a nucleophile. In this sense, the concept of electrophilicity, *i.e.* the relative reactivity of an electrophilic reagent, is, according to the IUPAC Goldbook,[3] directly related to Lewis acidity. Despite that, whereas Lewis acidity is a thermodynamic quantity (measured by relative equilibrium constants), electrophilicity is assumed to be a kinetic quantity (estimated from relative rate constants).

From an experimental point of view, the estimation and/or quantification of the relative electrophilicity of a system was challenging until the pioneering work by Mayr and co-workers,[4] who introduced nucleophilicity/electrophilicity scales based on the experimental rate constants for a large series of polar reactions. Thus, their famous equation $\log k = s_N(N + E)$, characterizes electrophiles by the parameter E (electrophilicity) and nucleophiles by two solvent-dependent quantities, N (nucleophilicity) and s_N (susceptibility).

From a theoretical point of view, electrophilicity is mostly quantified by means of the so-called Conceptual Density Functional Theory (CDFT) developed by Parr and Yang.[5] Within the CDFT approach, the electrophilicity index (ω)[6] is defined in terms of the chemical hardness (η)[5,7] and the chemical potential (μ)[5,7] as:

$$\omega = \mu^2/2\eta$$

where $\mu = \frac{1}{2}(\varepsilon_{LUMO} + \varepsilon_{HOMO})$ and $\eta = \varepsilon_{LUMO} - \varepsilon_{HOMO}$. Therefore, the electrophilicity of a system exclusively depends on the energy of its frontier molecular orbitals (FMOs) computed at its equilibrium geometry.[8,9] However, this is a rather crude assumption because electrophilicity, as a kinetic concept, is determined by the mutual interaction between the electrophile and nucleophile along the reaction coordinate, and particularly, at the transition state region, where the starting materials are significantly distorted and thus, their MOs may change quite a bit. For this reason, it is not surprising that the computed global or local ω values do not correlate with the experimental Mayr' E values in many instances, and particularly, for ketones, one of the most frequently used electrophiles in synthesis, as reported recently by Mayr and co-workers.[10]

This finding therefore suggests that the widely accepted orbital control (especially, the energy of the π*(C=O) molecular orbital)[11] is not the main factor governing the relative electrophilicity of carbonyl compounds. A similar finding was found by us recently in a completely different context but also involving carbonyl groups.[12,13] It was found that the catalysis of various reactions, such as Diels–Alder or Michael addition, is not, as widely accepted, caused by enhancing FMO interactions, but by a significant reduction in the Pauli repulsion between the key occupied molecular orbitals of the reactants, as revealed by the Activation Strain Model (ASM)[14] of reactivity and energy decomposition analysis (EDA) methods.[15] The lack of fundamental knowledge on the ultimate factors controlling the electrophilicity of carbonyl compounds, especially ketones and aldehydes,[10] prompted us to apply our combined ASM-EDA approach to reveal the origin of the relative electrophilicity of carbonyl compounds.

[a]*Department of Chemistry and Pharmaceutical Sciences, AIMMS, Vrije Universiteit Amsterdam, The Netherlands. E-mail: f.m.bickelhaupt@vu.nl*

[b]*Institute for Molecules and Materials (IMM), Radboud University, Nijmegen, The Netherlands*

[c]*Department of Chemical Sciences, University of Johannesburg, South Africa*

[d]*Departamento de Química Orgánica, Centro de Innovación en Química Avanzada (ORFEO-CINQA), Facultad de Ciencias Químicas, Universidad Complutense de Madrid Ciudad Universitaria, 28040-Madrid, Spain. E-mail: israel@quim.ucm.es*

† Electronic supplementary information (ESI) available: Cartesian coordinates and energies of all the species discussed in the text. See DOI: https://doi.org/10.1039/d3sc05595g

Results and discussion

We first focused on the relative electrophilicity of cyclohexanones, species experimentally investigated by Mayr and co-workers.[10] By studying the so-called Darzens condensation,[16] a process related to the useful Corey–Chaykovsky epoxidation,[17] the authors found that electrophilicity of the parent cyclohexanone ($E = -19.9$) increases with the presence of substituents in 4-relative position to the carbonyl group (Table 1). In particular, the cyclohexanones where the CH_2 group in position 4 was replaced by an oxygen or sulphur atom were found to exhibit an enhanced electrophilicity ($E = -17.9$ and -16.9, respectively).

The reasons behind the electrophilicity trend shown in Table 1 are however essentially unknown so far. Therefore, we decided to explore the simple addition of cyanide (CN^-) to the cyclohexanones **1** depicted in Table 1. This particular nucleophile was selected because is a potent nucleophile ($N = 16.27$ in the Mayr's scale)[4d] and its contribution to the total strain is practically negligible. In all cases, the process leads to the formation of the corresponding cyanohydrin adducts through transition states where the CN^- nucleophile follows the expected Bürgi–Dunitz angle (*ca.* 110°).[18] Interestingly, the computed activation barriers follow the same trend as the electrophilic E values, confirming that the substitution at the 4-position enhances the electrophilicity of the parent cyclohexanone (particularly for **1-O** and **1-S**, which exhibit rather low activation barriers). At variance, and in agreement with the findings by Mayr and co-workers,[10] no correlation was found between the computed barriers and the Parr's global electrophilicity indices, ω. No correlation was found either when using the local electrophilicity indices at the carbonyl carbon atom (see Table 1).[10]

To understand the origins of the enhanced reactivity of substituted cyclohexanones with respect to the parent system, we applied next the Activation Strain Model (ASM)[14] of reactivity. To this end, we compared the cyanide addition reactions involving the extreme situations represented by cyclohexanone **1-CH$_2$** and its sulphur-substituted counterpart **1-S**. Fig. 1 shows the corresponding Activation Strain Diagrams (ASDs) for both transformations from the early stages of the processes up to the corresponding transition states projected onto the (O=)C···C(N) bond-forming distance. From the data in Fig. 1, it becomes evident that the higher reactivity of **1-S** is not at all due to the strain term, which is nearly identical for both reactions but derives exclusively from a stronger interaction between the reagents along the entire reaction coordinate. The crucial role of the interaction between the reagents is further confirmed by the good linear relationship (correlation coefficient of 0.96) observed when plotting the computed barriers *versus* the ΔE_{int} values (computed at the same consistent C···C bond-forming distance of 2.06 Å).

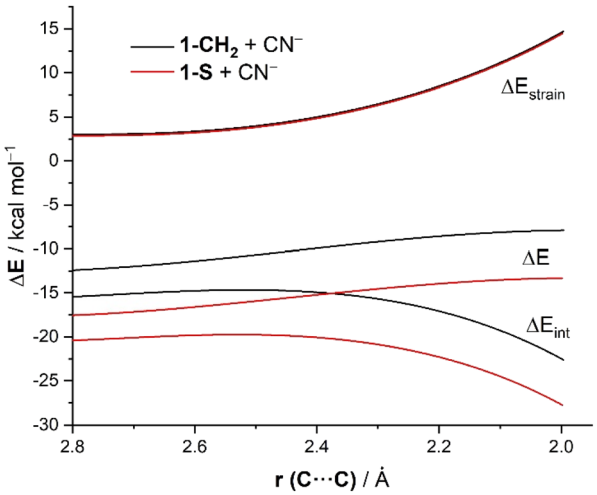

Fig. 1 Comparative ASDs of the reaction between CN^- and **1-CH$_2$** (black lines) and **1-S** (red lines) projected onto the C···C bond-forming distance and referred to the isolated reactants. All data have been computed at the ZORA-M06-2X/TZ2P//M06-2X/6-311+G* level.

The stronger interaction computed for the processes involving the substituted cyclohexanones in comparison with the parent system may be initially traced to the stabilization of the key π*(C=O) molecular orbital. For instance, whereas the energy of this π*–LUMO in **1-CH$_2$** is 0.37 eV, a lower value was computed for the more reactive systems **1-O** (0.24 eV) or **1-S** (0.19 eV). This should be translated into stronger orbital interactions in these substituted systems. However, from the Energy Decomposition Analysis (EDA) data in Table 1, computed at the same consistent C···C bond-forming distance, it becomes clear that the total orbital interaction term, ΔE_{orb}, remains nearly constant (*ca.* −55.5 kcal mol^{-1}, average). This indicates that the HOMO(CN^-) → π*–LUMO(C=O) interaction, is not, as

Table 1 Electrophilicities (E) and global electrophilicity indexes (ω) for cyclohexanones **1** together with reaction barriers ($\Delta G^{\ddagger}$) and EDA terms (in kcal mol^{-1}, computed at the ZORA-M06-2X/TZ2P//M06-2X/6-311+G* level) of the reactions of **1** and CN^-

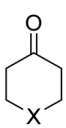

1-X	E^a	ω^b	$\Delta G^{\ddagger}$	$\Delta E_{int}{}^c$	$\Delta E_{Pauli}{}^c$	$\Delta V_{elstat}{}^c$	$\Delta E_{orb}{}^c$	$\Delta E_{orb}(\rho 1)^c$
1-CH$_2$	−19.9	0.93 (0.15)	6.5	−20.7	94.5	−60.0	−55.2	−47.1
1-NMe	−18.4	0.88 (0.15)	5.1	−22.5	95.2	−62.1	−55.5	−47.2
1-C(O$_2$C$_2$H$_4$)	−18.2	0.92 (0.15)	5.4	−22.8	94.8	−61.8	−55.8	−46.9
1-O	−17.9	1.01 (0.18)	2.7	−24.5	95.5	−64.9	−55.0	−47.3
1-S	−16.9	0.92 (0.19)	1.0	−25.9	95.6	−65.7	−55.9	−47.4
1-PMe	n.d.[d]	0.89 (n.d.)[d]	2.8	−24.3	95.0	−62.8	−56.4	−47.4
1-C(Me$_2$)	n.d.[d]	0.93 (n.d.)[d]	5.8	−21.4	95.0	−60.4	−56.0	−47.2

[a] Values measured by Mayr and co-workers (see ref. 10). [b] Computed at the M06-2X/TZ2P//M06-2X/6-311+G* level. Values within parentheses refer to the local electrophilicity index (ω_c) taken from ref. 10. [c] Computed at the same consistent C···C bond-forming distance of 2.06 Å. [d] Not determined.

traditionally assumed, the main factor controlling the interaction between the reactants and explains why the Parr's ω values fail to measure the electrophilicity of these cyclic ketones.

The same conclusion can be drawn by analyzing the evolution of the EDA terms along the entire reaction coordinate (*i.e.* from the beginning of the process up to the corresponding transition states). As shown in Fig. 2, the stronger interaction computed for the addition of cyanide to **1-S** in comparison to the analogous process involving the parent cyclohexanone **1-CH_2** is due neither to the Pauli repulsion nor the orbital interactions, which are nearly identical for both processes, but exclusively to stronger electrostatic attractions between the reactants along the entire reaction coordinate. The ΔV_{elstat} term is not only the dominant attractive term but also its evolution parallels that of the total interaction energy. Indeed, a very good linear correlation (correlation coefficient of 0.93) was found when plotting the ΔE_{int} term *vs.* the ΔV_{elstat} (at the same consistent C···C bond-forming distance of 2.06 Å). Therefore, the relative electrophilicity of the studied cyclohexanones seems to be exclusively defined, not by orbital interactions as traditionally considered, but by the electrostatic interactions between the electrophile and the nucleophile.

The origin of the counterintuitive computed nearly identical orbital interactions for all the considered cyclohexanones deserves further analysis. We first applied the Natural Orbital from Chemical Valence (NOCV)[19] extension of the EDA method to not only visualize but also quantify the main orbital interactions involved in the considered nucleophilic addition. As expected, the EDA-NOCV method indicates that the main contribution to the total ΔE_{orb} term (>90%) comes from the HOMO(nucleophile) → π*–LUMO(C=O) molecular orbital interaction (Fig. 3). Interestingly, the corresponding associated stabilization energies, $\Delta E_{orb}(\rho 1)$, are nearly identical for all processes (see Table 1 and Fig. 3 for the values of the representative reactions involving **1-CH_2** and **1-S** at the same consistent C···C bond-forming distance). This is mainly due to the rather similar π*–LUMO(C=O) orbital energy (see above) and the nearly identical ⟨HOMO(CN^-)|π*–LUMO(C=O)⟩ overlap ($S = 0.33$ and 0.34 for **1-CH_2** and **1-S**; values computed at the same point r(C···C) along the reaction coordinate). As a result, the total electronic charge transferred from the HOMO(CN^-) to the π*–LUMO(C=O) hardly varies in all systems (0.646e *vs.* 0.647e for **1-CH_2** and **1-S**, respectively, at the same C···C bond-forming distance). This circumstance renders the molecular orbital interaction and, consequently, ω irrelevant in defining the actually measured or computed relative electrophilicity of the considered cyclohexanones.

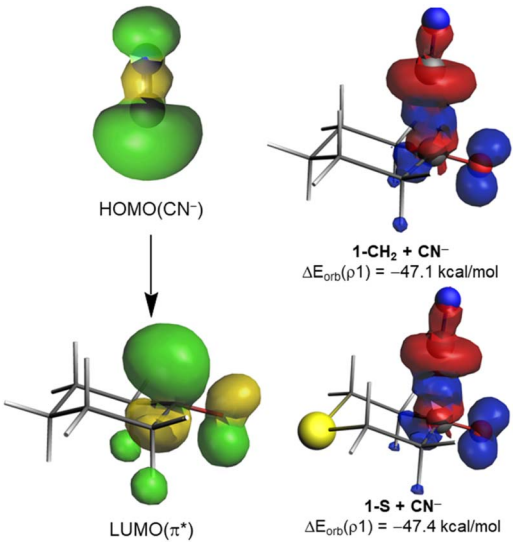

Fig. 3 Deformation densities $\rho 1$ and associated molecular orbitals of the most important orbital interaction $\Delta E_{orb}(\rho 1)$ in the reaction between CN^- and **1-CH_2** or **1-S**. The color code used to represent the flow of charge is red → blue. All data have been computed at the ZORA-M06-2X/TZ2P//M06-2X/6-311+G* level.

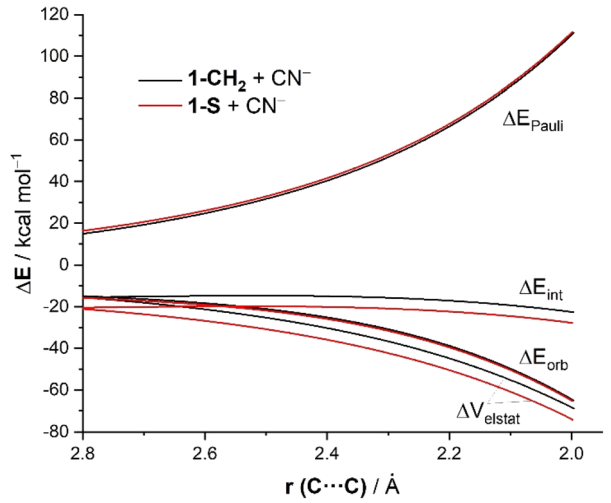

Fig. 2 Comparative EDAs of the reaction between CN^- and **1-CH_2** or **1-S** projected onto the C···C bond-forming distance and referred to the isolated reactants. All data have been computed at the ZORA-M06-2X/TZ2P//M06-2X/6-311+G* level.

It is reasonable to assume that the above results might be biased due to the charged nature of the cyanide nucleophile. To check whether the electrostatic attractions also play a crucial role in analogous reactions involving neutral nucleophiles, we compared the processes involving **1-CH_2** and **1-S** with the ylide nucleophiles Me_2S=CH–CN ($N = 16.23$), Me_2S=CH–CO_2Me ($N = 15.85$) and Me_2S=CH–$p(NO_2)C_6H_4$ ($N = 18.42$), which present similar N values as cyanide.[4d] In addition, we also considered the negatively charged [Cl–CH–SO_2Ph]$^-$ nucleophile, used in the experiments involving these cyclohexanones,[10] because the negative charge is much more delocalized than in cyanide. From the data in Table 2, **1-S** is confirmed to be a better electrophile than **1-CH_2** according to the lower barriers computed for all the nucleophilic additions. Interestingly, regardless of the nucleophile the interaction energy between the electrophile and the nucleophile (computed at a consistent C···C bond-forming distance close to that of the corresponding transition states) is systematically stronger (*i.e.* more negative) for the processes involving **1-S**. Once again, it is found that even when neutral nucleophiles are involved, the crucial electrostatic term,

Table 2 Computed reaction barriers ($\Delta G^{\ddagger}$) and EDA terms (in kcal mol^{-1}, computed at the ZORA-M06-2X/TZ2P//M06-2X/6-311+G* level)[a] of the reactions of **1-CH$_2$** and **1-S** with different nucleophiles

System						
1-X	Nucleophile	$\Delta G^{\ddagger}$	ΔE_{int}	ΔE_{Pauli}	ΔV_{elstat}	ΔE_{orb}
1-CH$_2$	$Me_2S{=}CH{-}CN$	20.7	−21.4	180.5	−109.2	−92.7
1-S		19.6	−22.7	180.5	−109.7	−93.5
1-CH$_2$	$Me_2S{=}CH{-}CO_2Me$	24.8	−23.0	180.9	−109.8	−94.1
1-S		23.7	−24.6	181.7	−111.0	−95.2
1-CH$_2$	$Me_2S{=}CH{-}p(NO_2)C_6H_4$	19.6	−19.6	138.6	−87.7	−70.4
1-S		18.0	−21.6	139.9	−89.2	−72.2
1-CH$_2$	$[Cl{-}CH{-}SO_2Ph]^-$	10.3	−22.4	141.8	−87.7	−77.4
1-S		5.1	−27.6	143.5	−91.9	−49.6

[a] Computed at the same consistent C···C bond-forming distance (*i.e.* the distance in the transition state of the **1-S** process).

ΔV_{elstat}, is not only the major contribution to the total ΔE_{int} but is also comparatively more stabilizing for the reactions involving **1-S**. Therefore, these results further confirm the crucial role of electrostatic attractions in controlling the electrophilicity of these cyclohexanones.

The somehow unexpected close relationship between electrophilicity and electrostatic interactions prompted us to explore the generality of this finding. So, we decided to investigate the similar cyanide nucleophilic addition to a series of benzaldehydes differently substituted at the 4-position of the aryl ring. Similar to the analogous process involving cyclohexanones, in all cases the reaction affords the corresponding adduct through the respective transition states which again follow the expected Bürgi–Dunitz trajectory. In this transformation, we also located an initial reactant complex (**RC**) which lies below the separate reactants and has been therefore used as the reference level to compute the corresponding activation barriers (Fig. 4).

From the computed barriers gathered in Table 3, it appears that the presence of an electron-withdrawing group in the *para* position enhances the electrophilicity of the benzaldehyde whereas electron-donor groups provoke the opposite effect, which confirms expectations based on the corresponding σ-Hammett constants.[20] In addition, we find that the C···C bond-forming distance in the corresponding transition states becomes systematically longer from **2-NMe$_2$** (r = 2.073 Å) to **2-NO$_2$** (r = 2.232 Å), which indicates that the transition state is reached earlier as the acceptor ability of the substituent increases. In line with this, we establish an excellent linear correlation between the computed barriers and the C···C bond-forming distance in the TS (correlation coefficient of 0.99). These reactions, therefore, follow the Hammond–Leffer postulate.[21]

To quantitatively understand the reactivity trend observed in the cyanide addition to benzaldehydes, we have applied once again the ASM of reactivity. To this end, we focus on three representative processes involving unsubstituted (**2-H**), electron-donor substituted (**2-NMe$_2$**), and electron-acceptor substituted (**2-NO$_2$**) benzaldehydes. Fig. 5 shows the corresponding ASDs for these reactions once again from the beginning of the process up to the corresponding transition states and projected onto the forming (O=)C···C(N) bond-forming distance. As shown in Fig. 5, the enhanced reactivity of *p*-NO_2–benzaldehyde **2-NO$_2$** in comparison with the parent benzaldehyde **2-H** is again solely due to the stronger interaction energy between the reactants along the entire reaction coordinate. The deformation strain energy, ΔE_{strain}, is nearly identical for both transformations. The reaction involving *p*-NMe_2–benzaldehyde **2-NMe$_2$** exhibits the weakest, *i.e.*, the least stabilizing ΔE_{int} along the entire series which, together with a more destabilizing strain energy, results in a higher barrier and thus a reduced reactivity (*i.e.*, electrophilicity) for this system. The crucial role of the interaction between the reagents is further confirmed by the excellent linear correlation (correlation coefficient of 0.99, see Fig. 6) between the computed barriers and the ΔE_{int} values, computed at the same consistent C···C bond-forming distance of 2.232 Å (*i.e.*, the value for the transition state involving **2-NO$_2$**).

For this particular transformation, we found that the computed electrophilicity indices, ω, do follow the same trend

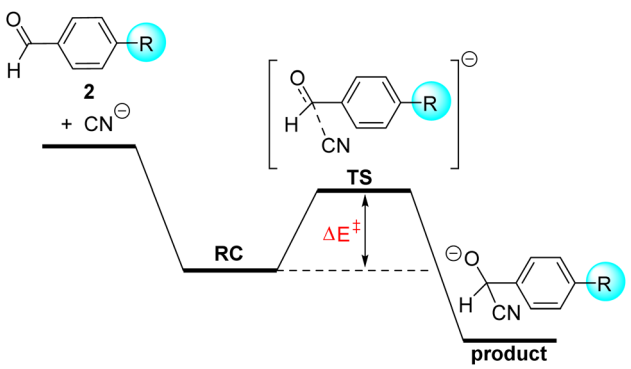

Fig. 4 Schematic reaction profile for the nucleophilic addition reaction of CN^- to benzaldehydes **2**.

Table 3 Computed global electrophilicity indexes (ω) for benzaldehydes **2** together with reaction barriers ($\Delta E^{\ddagger}$) and EDA terms (in kcal mol^{-1}, computed at the ZORA-M06-2X/TZ2P//M06-2X/6-311+G* level)[a] of the reactions of **2** and CN^-

System							
2-R	$\Delta E^{\ddagger}$	ω	ΔE_{strain}	ΔE_{int}	ΔE_{Pauli}	ΔV_{elstat}	ΔE_{orb} ($\Delta E_{orb}(\rho 1)$)
2-NMe$_2$	9.0	1.1	9.1	−13.5	58.9	−34.0	−38.3 (−33.7)
2-*t*Bu	8.6	1.4	6.3	−15.1	58.8	−35.3	−38.6 (−34.3)
2-Me	8.4	1.5	5.9	−14.8	58.8	−35.5	−38.1 (−34.2)
2-H	8.2	1.6	6.1	−15.8	58.7	−36.6	−37.8 (−34.4)
2-Br	7.1	1.8	6.2	−20.0	59.1	−40.0	−39.2 (−35.1)
2-CF$_3$	5.9	1.9	6.3	−22.5	59.2	−42.7	−39.1 (−35.8)
2-CN	5.3	2.2	5.7	−24.9	59.6	−44.4	−40.0 (−36.4)
2-NO$_2$	4.9	2.5	5.9	−26.3	59.8	−45.7	−40.4 (−37.0)

[a] Computed at the same consistent C···C bond-forming distance of 2.232 Å

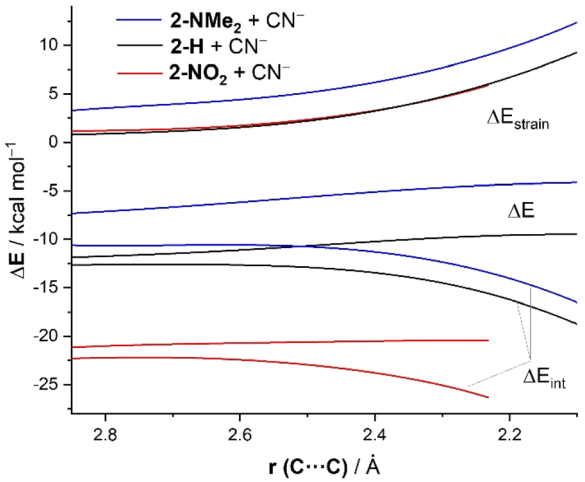

Fig. 5 Comparative ASDs of the reaction between CN^- and **2-NMe$_2$** (blue lines), **2-H** (black lines) and **2-NO$_2$** (red lines) projected onto the C···C bond-forming distance and referred to the isolated reactants. All data have been computed at the ZORA-M06-2X/TZ2P//M06-2X/6-311+G* level.

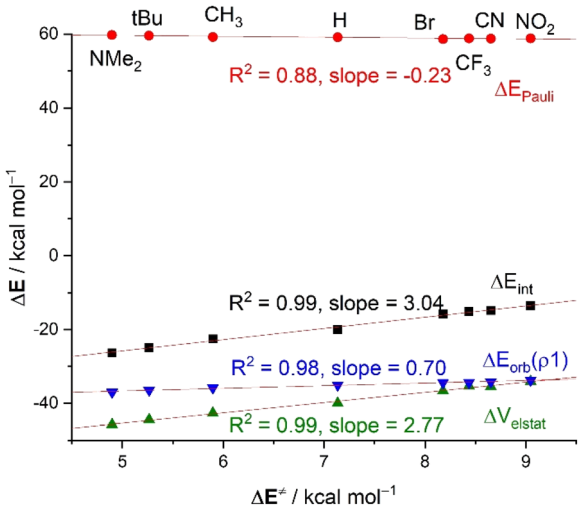

Fig. 6 Plot of the activation energies ($\Delta E^{\ddagger}$) and the EDA terms for the reactions of CN^- and benzaldehydes **2** (at a consistent C···C bond-forming distance of 2.232 Å). All data have been computed at the ZORA-M06-2X/TZ2P//M06-2X/6-311+G* level.

as the activation barriers (correlation coefficient of 0.92), which would suggest that the electrophilicity of the considered benzaldehydes could be defined by the energy of their FMOs. This is in line with the computed key HOMO(CN^-) → π*–LUMO(C═O) molecular orbital interactions, reflected by the $\Delta E_{orb}(\rho 1)$ term, which also follows the same trend, *i.e.*, this HOMO–LUMO interaction becomes stronger as the electron-withdrawing ability of the substituent increases (see Table 3). As a result, we find in this case a good correlation between the barriers and $\Delta E_{orb}(\rho 1)$ term ($R^2 = 0.98$, Fig. 6). This can be initially ascribed to the stabilization of the π*(C═O)–LUMO (*e.g.*, $\varepsilon_{LUMO} = -0.87$, -1.14 and -2.44 eV, for **2-NMe$_2$**, **2-H** and **2-NO$_2$**, respectively, at the same consistent point *r*(C···C) along the reaction coordinate) and is once again related to the total electronic charge transferred from the nucleophile to the π*(C═O) orbital of the substrate, which clearly increases from **2-NMe$_2$** (0.600*e*) to **2-NO$_2$** (0.632*e*). Despite that, the variation in the $\Delta E_{orb}(\rho 1)$ term along the series is not remarkable (*ca.* 3 kcal mol^{-1}) which is reflected in the low slope (0.70) of the corresponding correlation line. This indicates a low sensitivity of the reactivity (*i.e.* electrophilicity) with the FMO interactions. The same holds for the ΔE_{Pauli} term, which hardly varies along the entire series either (Fig. 6). This is due to the overlap between the key occupied molecular orbitals of both reactants, in particular, the ⟨π(C═O)(**2**)|HOMO(CN^-)⟩, which changes not that much when comparing the extreme situations involving **2-NMe$_2$** ($S = 0.06$) with **2-NO$_2$** ($S = 0.08$).

At variance, the electrostatic attraction is again the main factor controlling both, the magnitude of, and the trend in, the interaction ΔE_{int} between the deformed reactants. Indeed, as clearly shown in Fig. 6, the ΔV_{elstat} values parallel the ΔE_{int} values, which is translated into a very good correlation between the computed barriers and the ΔV_{elstat} term (correlation coefficient of 0.99). In this case, the computed high slope of 2.77 indicates a much higher sensitivity of the actual electrophilicity for the electrostatic interactions.

The same conclusion can be drawn when plotting the evolution of the EDA terms along the entire reaction coordinate for the processes involving **2-NMe$_2$**, **2-H** and **2-NO$_2$**. As graphically shown in Fig. 7, the Pauli repulsion term is nearly identical in all the reactions. At variance, the orbital interactions are only slightly stronger for the process involving **2-NO$_2$** as compared to the analogous reaction involving **2-NMe$_2$** or **2-H**. However, the electrostatic attraction (ΔV_{elstat}) becomes the decisive factor leading to the observed trend in ΔE_{int} (**2-NO$_2$** > **2-H** > **2-NMe$_2$**). Thus, ΔV_{elstat} steadily strengthens from **2-NO$_2$** to **2-H** and to **2-**

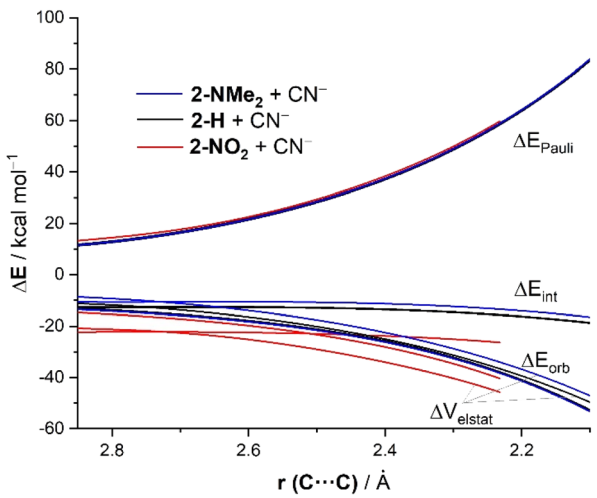

Fig. 7 Comparative EDAs of the reaction between CN^- and **2-NMe$_2$** (blue lines), **2-H** (black lines) and **2-NO$_2$** (red lines) projected onto the C···C bond-forming distance and referred to the isolated reactants. All data have been computed at the ZORA-M06-2X/TZ2P//M06-2X/6-311+G* level.

NMe$_2$ and, in this way, causes the same trend in ΔE_{int} and, ultimately, in the actual relative electrophilicity of these benzaldehydes as reflected by $\Delta E^{\ddagger}$.[22]

The trend in the key term, ΔV_{elstat}, which as commented above controls the reactivity of the system, can be directly related to the variation of the charge at the carbonyl carbon atom. The latter becomes more positive with the higher electron-withdrawing capacity of the substituent. For instance, the computed Hirshfeld charge at this carbonyl carbon atom steadily increases from +0.119 in **2-NMe$_2$** to +0.132 in **2-NO$_2$**. For this reason, an excellent linear correlation ($R^2 = 0.96$) arises between the activation barrier and the charge of the carbonyl carbon atom of the considered benzaldehydes (Fig. 8).

Conclusions

According to our activation strain and quantitative MO analyses, the electrophilicity of our model organic carbonyls (*i.e.* cyclohexanones or benzaldehydes) is mainly determined by the electrostatic attractions between the electrophile and nucleophile reactants along the reaction coordinate. For the particular case of *p*-substituted benzaldehydes, it is found that the relative electrophilicity is related to the charge on the carbonylic carbon atom, which directly depends on the electron-withdrawing or donating power of the *para*-substituent. The more positive the carbonylic carbon atom, the more stabilizing the electrostatic interaction with the CN^- nucleophile and, thus, the lower the activation energy. At variance, the relative electrophilicity of these benzaldehydes exhibits a low sensitivity with the FMO interactions, although the key π*(C═O) MO becomes more and more stabilized with the electron-withdrawing ability of the substituent.

This finding becomes even more evident in the cyclohexanones series considered herein, as for these systems, the key π*(C═O) remains almost constant, which is translated into nearly identical FMO interactions. As a consequence, the trend in the relative electrophilicity of these systems greatly deviates from the trend predicted by the widely used ω index, as confirmed experimentally.[9]

Our finding, *i.e.* the electrostatic interactions as the main factor governing the electrophilicity of carbonyl compounds, therefore contrasts with, and replaces the traditional rationalization of the electrophilicity trends based exclusively on the FMO interactions, at least for the series of nucleophiles considered in this study.

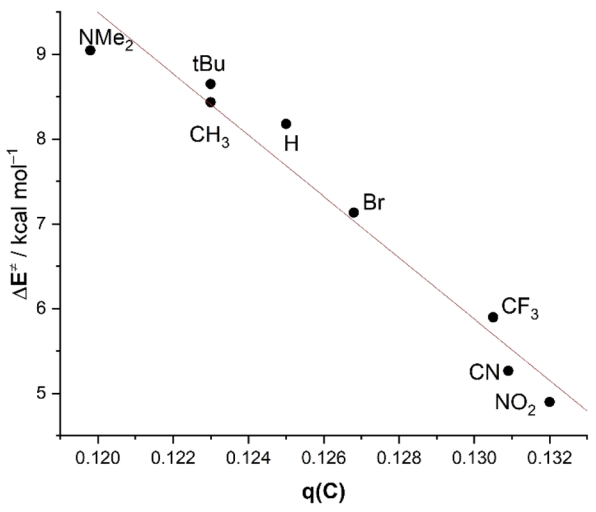

Fig. 8 Plot of the activation energies ($\Delta E^{\ddagger}$) *versus* the computed Hirshfeld charges of the carbonyl carbon atom of benzaldehydes **2** (at a consistent C···C bond-forming distance of 2.232 Å). All data have been computed at the ZORA-M06-2X/TZ2P//M06-2X/6-311+G* level.

Computational details

Geometry optimizations of the molecules were performed without symmetry constraints using the Gaussian16 (RevB.01) suite of program[23] at the M06-2X[24]/6-311+G* level. Reactants and adducts were characterized by frequency calculations and have positive definite Hessian matrices. Transition states show only one negative eigenvalue in their diagonalized force constant matrices, and their associated eigenvectors were confirmed to correspond to the motion along the reaction coordinate under consideration using the Intrinsic Reaction Coordinate (IRC) method.[25]

Activation strain model (ASM) of reactivity and energy decomposition analysis (EDA) methods

Within the ASM method,[14] the potential energy surface $\Delta E(\zeta)$ is decomposed along the reaction coordinate, ζ, into two contributions, namely the strain $\Delta E_{strain}(\zeta)$ associated with the deformation (or distortion) required by the individual reactants during the process and the interaction $\Delta E_{int}(\zeta)$ between these increasingly deformed reactants:

$$\Delta E(\zeta) = \Delta E_{strain}(\zeta) + \Delta E_{int}(\zeta)$$

Within the EDA method,[14] the interaction energy can be further decomposed into the following chemically meaningful terms:

$$\Delta E_{int}(\zeta) = \Delta V_{elstat}(\zeta) + \Delta E_{Pauli}(\zeta) + \Delta E_{orb}(\zeta)$$

The term ΔV_{elstat} corresponds to the classical electrostatic interaction between the unperturbed charge distributions of the deformed reactants and is usually attractive. The Pauli repulsion ΔE_{Pauli} comprises the destabilizing interactions between occupied orbitals and is responsible for any steric repulsion. The orbital interaction ΔE_{orb} accounts for bond pair formation, charge transfer (interaction between occupied orbitals on one moiety with unoccupied orbitals on the other, including HOMO–LUMO interactions), and polarization (empty-occupied orbital mixing on one fragment due to the presence of another fragment). Moreover, the NOCV (Natural Orbital for Chemical Valence)[19] extension of the EDA method has been also used to further partition the ΔE_{orb} term. The EDA-NOCV approach

provides pairwise energy contributions for each pair of interacting orbitals to the total bond energy.

The program package ADF[26] was used for EDA calculations using the optimized M06-2X/6-311+G* geometries at the same DFT level in conjunction with a triple-ζ-quality basis set using uncontracted slater-type orbitals (STOs) augmented by two sets of polarization functions with a frozen-core approximation for the core electrons.[27] Auxiliary sets of s, p, d, f, and g STOs were used to fit the molecular densities and to represent the Coulomb and exchange potentials accurately in each SCF cycle.[28] Scalar relativistic effects were incorporated by applying the zeroth-order regular approximation (ZORA).[29] This level of theory is denoted ZORA-M06-2X/TZ2P//M06-2X/6-311+G*.

Data availability

Cartesian coordinates and energies of all species discussed in the text are available in the ESI.†

Author contributions

I. F. initial conceptualization, calculations and manuscript writing. F. M. B. discussion, conceptualization, and manuscript writing.

Conflicts of interest

There are no conflicts to declare.

Acknowledgements

This work was supported by the Spanish MCIN/AEI/10.13039/501100011033 (Grants PID2019-106184GB-I00, PID2022-139318NB-I00 and RED2022-134287-T) and the Dutch Research Council (NWO).

Notes and references

1 C. K. Ingold, *J. Chem. Soc. D*, 1933, 1120.
2 (*a*) G. N. Lewis and P. Wheeler, *Zeitschrift für Physikalische Chemie*, 1906, **56U**, 179; (*b*) G. N. Lewis, *J. Am. Chem. Soc.*, 1916, **38**, 762.
3 IUPAC, *Compendium of Chemical Terminology*, the "Gold Book", compiled by A. D. McNaught and A. Wilkinson, Blackwell Scientific Publications, Oxford, 2nd edn, 1997, online version (2019–) created by S. J. Chalk, DOI: **10.1351/goldbook**.
4 (*a*) H. Mayr, T. Bug, M. F. Gotta, N. Hering, B. Irrgang, B. Janker, B. Kempf, R. Loos, A. R. Ofial, G. Remennikov and H. Schimmel, *J. Am. Chem. Soc.*, 2001, **123**, 9500; (*b*) R. Lucius, R. Loos and H. Mayr, *Angew. Chem., Int. Ed.*, 2002, **41**, 91; (*c*) H. Mayr, B. Kempf and A. R. Ofial, *Acc. Chem. Res.*, 2003, **36**, 66; (*d*) For a database of nucleophilicity parameters N/s_N, and electrophilicity parameters E, check the link: **https://www.cup.lmu.de/oc/mayr/reaktionsdatenbank2/**.
5 (*a*) R. G. Parr and W. Yang, *Density-Functional Theory of Atoms and Molecules*, Oxford University Press, Clarendon Press, New York, 1989; (*b*) P. Geerlings, F. de Proft and W. Langenaeker, *Chem. Rev.*, 2003, **103**, 1793.
6 R. G. Parr, L. V. Szentpály and S. Liu, *J. Am. Chem. Soc.*, 1999, **121**, 1922.
7 R. G. Parr and R. G. Pearson, *J. Am. Chem. Soc.*, 1983, **105**, 7512.
8 P. K. Chattaraj, U. Sarkar and D. R. Roy, *Chem. Rev.*, 2006, **106**, 2065.
9 There are in addition other alternative definitions in CDFT using the finite difference approximation,(*a*) E. Chamorro, P. K. Chattara and P. Fuentealba, *J. Phys. Chem. A*, 2003, **107**, 7068; second-order Taylor expansions of the energy, (*b*) J. L. Gázquez, A. Cedillo and A. Vela, *J. Phys. Chem. A*, 2007, **111**, 1966; and advances including the two-parabola model, (*c*) A. U. Orozco-Valencia, J. L. Gázquez and A. Vela, *J. Phys. Chem. A*, 2018, **122**, 1796. See also, (*d*) E. Chamorro, M. Duque-Noreña and P. Pérez, *J. Mol. Struct.: THEOCHEM*, 2009, **896**, 73.
10 Z. Li, H. Jangra, Q. Chen, P. Mayer, A. R. Ofial, H. Zipse and H. Mayr, *J. Am. Chem. Soc.*, 2018, **140**, 5500.
11 See, for instance: (*a*) J. Clayden, N. Greeves, S. Warren and P. Wothers, *Organic Chemistry*, Oxford University Press, London, England, 2nd edn, 2014; (*b*) E. V. Anslyn and D. A. Dougherty, *Modern Physical Organic Chemistry*, University Science Books, 2006.
12 (*a*) T. A. Hamlin, I. Fernández and F. M. Bickelhaupt, *Angew. Chem., Int. Ed.*, 2019, **58**, 8922; (*b*) P. Vermeeren, T. A. Hamlin, I. Fernández and F. M. Bickelhaupt, *Angew. Chem., Int. Ed.*, 2020, **59**, 6201; (*c*) P. Vermeeren, T. A. Hamlin, I. Fernández and F. M. Bickelhaupt, *Chem. Sci.*, 2020, **11**, 8105.
13 T. A. Hamlin, F. M. Bickelhaupt and I. Fernández, *Acc. Chem. Res.*, 2021, **54**, 1972.
14 (*a*) I. Fernández and F. M. Bickelhaupt, *Chem. Soc. Rev.*, 2014, **43**, 4953; (*b*) P. Vermeeren, S. C. C. van der Lubbe, C. Fonseca Guerra, F. M. Bickelhaupt and T. A. Hamlin, *Nat. Protoc.*, 2020, **15**, 649; (*c*) F. M. Bickelhaupt and K. N. Houk, *Angew. Chem., Int. Ed.*, 2017, **56**, 10070. See also; (*d*) I. Fernández, in *Discovering the Future of Molecular Sciences*, ed. B. Pignataro, Wiley-VCH, Weinheim, 2014, pp. 165–187; (*e*) F. M. Bickelhaupt, *J. Comput. Chem.*, 1999, **20**, 114–128.
15 For reviews on the EDA method, see:(*a*) F. M. Bickelhaupt and E. J. Baerends, in *Reviews in Computational Chemistry*, ed. K. B. Lipkowitz and D. B. Boyd, Wiley-VCH, New York, 2000, vol. 15, pp. 1–86; (*b*) I. Fernández, in *Applied Theoretical Organic Chemistry*, ed. D. J. Tantillo, World Scientific, New Jersey, 2018, pp. 191–226.
16 (*a*) G. Darzens, *Comptes Rendus*, 1904, **139**, 1214; (*b*) G. Darzens, *Comptes Rendus*, 1905, **141**, 766; (*c*) G. Darzens, *Comptes Rendus*, 1906, **142**, 214; (*d*) G. Darzens and P. Lefébure, *Comptes Rendus*, 1906, **142**, 714.
17 (*a*) E. J. Corey and M. Chaykovsky, *J. Am. Chem. Soc.*, 1965, **87**, 1353; (*b*) A. W. Johnson and R. B. LaCount, *J. Am. Chem. Soc.*, 1961, **83**, 417.

18 For recent studies by us on the origin of the Bürgi-Dunitz angle in nucleophilic additions to carbonyl groups, see:(*a*) H. A. Rodríguez, F. M. Bickelhaupt and I. Fernández, *ChemPhysChem*, 2023, **24**, e202300379; (*b*) I. Fernández, F. M. Bickelhaupt and D. Svatunek, *J. Chem. Theory Comput.*, 2023, **19**, 7300.

19 M. P. Mitoraj, A. Michalak and T. Ziegler, *J. Chem. Theory Comput.*, 2009, **5**, 962.

20 (*a*) L. P. Hammett, *Chem. Rev.*, 1935, **17**, 125; (*b*) L. P. Hammett, *Physical Organic Chemistry*, McGraw-Hill, New York, 2nd edn, 1970. For studies using the EDA method to understand substituent effects, see also: (*c*) I. Fernández and G. Frenking, *J. Org. Chem.*, 2006, **71**, 2251; (*d*) O. A. Stasyuk, H. Szatylowicz, T. M. Krygowski and C. Fonseca Guerra, *Phys. Chem. Chem. Phys.*, 2016, **18**, 11624.

21 (*a*) G. S. Hammond, *J. Am. Chem. Soc.*, 1955, **77**, 334; (*b*) A. Pross, *Theoretical and Physical Principles in Organic Reactivity*, Wiley, Hoboken, 1995.

22 The same trend is found when considering solvent effects in the calculations. At the COSMO-ZORA-M06-2X/TZ2P//PCM(CH_2Cl_2)M06-2X/6-311+G* level, the ΔV_{elstat} term increases in the order −46.5 kcal mol^{-1} (**2-NMe$_2$**), −53.5 kcal mol^{-1} (**2-H**) and −64.7 kcal mol^{-1} (**2-NO$_2$**).

23 M. J. Frisch, G. W. Trucks, H. B. Schlegel, G. E. Scuseria, M. A. Robb, J. R. Cheeseman, G. Scalmani, V. Barone, G. A. Petersson, H. Nakatsuji, X. Li, M. Caricato, A. V. Marenich, J. Bloino, B. G. Janesko, R. Gomperts, B. Mennucci, H. P. Hratchian, J. V. Ortiz, A. F. Izmaylov, J. L. Sonnenberg, D. Williams-Young, F. Ding, F. Lipparini, F. Egidi, J. Goings, B. Peng, A. Petrone, T. Henderson, D. Ranasinghe, V. G. Zakrzewski, J. Gao, N. Rega, G. Zheng, W. Liang, M. Hada, M. Ehara, K. Toyota, R. Fukuda, J. Hasegawa, M. Ishida, T. Nakajima, Y. Honda, O. Kitao, H. Nakai, T. Vreven, K. Throssell, J. A. Montgomery Jr, J. E. Peralta, F. Ogliaro, M. J. Bearpark, J. J. Heyd, E. N. Brothers, K. N. Kudin, V. N. Staroverov, T. A. Keith, R. Kobayashi, J. Normand, K. Raghavachari, A. P. Rendell, J. C. Burant, S. S. Iyengar, J. Tomasi, M. Cossi, J. M. Millam, M. Klene, C. Adamo, R. Cammi, J. W. Ochterski, R. L. Martin, K. Morokuma, O. Farkas, J. B. Foresman, and D. J. Fox, *Gaussian 16, Revision, B.01*, Gaussian, Inc., Wallingford CT, 2016.

24 Y. Zhao and D. Truhlar, *Theor. Chem. Acc.*, 2008, **120**, 215.

25 C. Gonzalez and H. B. Schlegel, *J. Phys. Chem.*, 1990, **94**, 5523.

26 (*a*) G. te Velde, F. M. Bickelhaupt, E. J. Baerends, C. Fonseca Guerra, S. J. A. van Gisbergen, J. G. Snijders and T. Ziegler, *J. Comput. Chem.*, 2001, **22**, 931; (*b*) ADF2020, SCM, *Theoretical Chemistry*, Vrije Universiteit, Amsterdam, The Netherlands, **http://www.scm.com**.

27 J. G. Snijders, P. Vernooijs and E. J. Baerends, *At. Data Nucl. Data Tables*, 1981, **26**, 483.

28 J. Krijn and E. J. Baerends, *Fit Functions in the HFS-Method, Internal Report (in Dutch)*, Vrije Universiteit Amsterdam, The Netherlands, 1984.

29 (*a*) E. van Lenthe, E. J. Baerends and J. G. Snijders, *J. Chem. Phys.*, 1993, **99**, 4597; (*b*) E. van Lenthe, E. J. Baerends and J. G. Snijders, *J. Chem. Phys.*, 1994, **101**, 9783; (*c*) E. van Lenthe, A. Ehlers and E. J. Baerends, *J. Chem. Phys.*, 1999, **110**, 8943.